NANO LETTERS

Letter

pubs.acs.org/NanoLett

# Monolithic Electrically Injected Nanowire Array Edge-Emitting Laser on (001) Silicon

Thomas Frost,[†] Shafat Jahangir,[†] Ethan Stark,[†] Saniya Deshpande,[†] Arnab Hazari,[†] Chao Zhao,[‡] Boon S. Ooi,[‡] and Pallab Bhattacharya*[,†]

[†]Center for Photonics and Multiscale Nanomaterials, 1301 Beal Avenue, Department of Electrical Engineering and Computer Science, University of Michigan, Ann Arbor, Michigan 48109, United States

[‡] Division of Computer, Electrical and Mathematical Sciences and Engineering, King Abdullah University of Science and Technology (KAUST), Thuwal 23955-6900, Saudi Arabia

Supporting Information

**ABSTRACT:** A silicon-based laser, preferably electrically pumped, has long been a scientific and engineering goal. We demonstrate here, for the first time, an edge-emitting InGaN/GaN disk-in-nanowire array electrically pumped laser emitting in the green ($\lambda$ = 533 nm) on (001) silicon substrate. The devices display excellent dc and dynamic characteristics with values of threshold current density, differential gain, $T_0$ and small signal modulation bandwidth equal to 1.76 kA/cm$^2$, 3 × 10$^{-17}$ cm$^2$, 232 K, and 5.8 GHz respectively under continuous wave operation. Preliminary reliability measurements indicate a lifetime of 7000 h. The emission wavelength can be tuned by varying the alloy composition in the quantum disks. The monolithic nanowire laser on (001)Si can therefore address wide-ranging applications such as solid state lighting, displays, plastic fiber communication, medical diagnostics, and silicon photonics.

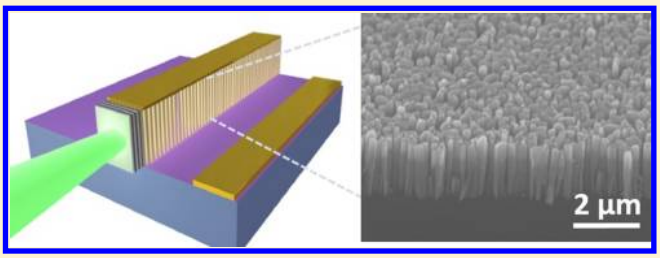


**KEYWORDS:** *Nanowire Laser, GaN Nanowire, Quantum Disk-in-Nanowire, Molecular Beam Eptiaxy*

A monolithic Si(001)-based electrically injected laser, preferably with low threshold, reasonably high output power, weak temperature dependence of the threshold, and large modal gain and differential gain, remains one of the biggest scientific and technological challenges to be overcome. Because silicon is an indirect bandgap semiconductor, free-carrier absorption, and nonradiative recombination processes prevent any significant light emission. A suitable monolithic silicon-based laser is central to the success of silicon photonics.[1−4] Additionally, if the laser can emit in the visible region, then the epitaxial growth of the common nitride-based laser heterostructures on overly expensive free-standing GaN substrates can be circumvented. Three routes for the integration of reliable and high-performance electrically pumped lasers with silicon technology are being explored. The first involves the direct epitaxy of III−V heterostructures on silicon. However, the large lattice mismatch leads to a high density of threading dislocations propagating into the active region. Furthermore, the formation of antiphase boundaries due to the polar/nonpolar nature of the epitaxy necessitates the use of misoriented substrates; generally Si(001) offcut 4° toward the [111] or [110] planes is used.[5−7] This is the greatest drawback of this method because Si CMOS technology on misoriented substrates is not favored. Nonetheless, high-performance InAs/GaAs quantum dot lasers on misoriented silicon with emission between 1.1 and 1.3 $\mu$m have been reported.[6−8] Various buffer layers are also being investigated for use in this approach.[3,9,10] As a second approach, an electrically pumped Ge-on-Si p-n-n heterojunction diode laser, with built-in tensile strain and heavy doping in the Ge layer, which allow direct radiative transitions in indirect bandgap Ge, has been demonstrated recently.[11] The reported power output and threshold current density at 15 °C are ∼1 mW and 280 kA/cm$^2$. The temperature dependence ($T_0$) and long-term reliability of this device have not been reported. The third, and perhaps the most common, technique has been to wafer bond the III−V laser heterostructure on a Si wafer.[4,12−16] Variations within this approach include guiding in the III−V heterostructures or in silicon via evanescent mode coupling. Microdisk lasers bonded on Si have also been reported.[17] However, the maximum bonding area is limited by the available size of GaAs or InP substrates.

III-nitride nanowires [(Al, Ga, In)N] can be grown catalyst-free on Si(001) substrates in the wurtzite crystalline form with the $c$ axis along the growth direction[18−28] and are promising in the development of visible light emitting diodes (LEDs) and lasers. III-nitride nanowires grown on silicon are relatively free of extended defects compared to bulk GaN grown on lattice mismatched substrates[27,28] because of the large surface-to-volume ratio and due to the formation of a 1−2 nm thick initial $SiN_x$ layer at the Si-GaN heterointerface, which behaves as a

Received: April 27, 2014
Revised: June 5, 2014

   dx.doi.org/10.1021/nl5015603 | Nano Lett. XXXX, XXX, XXX−XXX

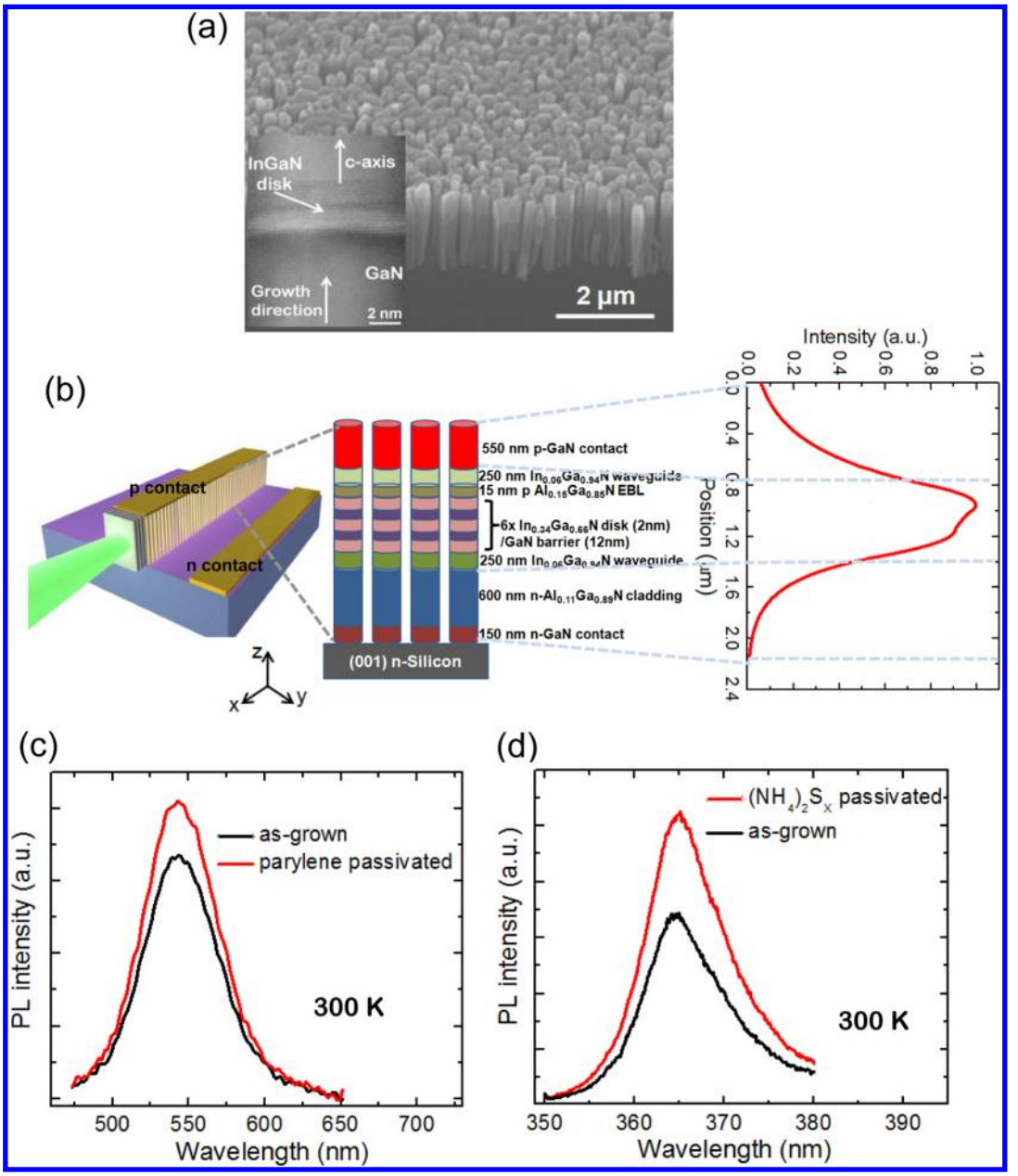


**Figure 1.** (a) Scanning electron microscope image of the as-grown disk-in-nanowire laser heterostructure grown by molecular beam epitaxy on (001) silicon substrate. The inset shows the high resolution transmission electron microscope image of one of the ∼2 nm thick $In_{0.34}Ga_{0.66}N$ disks with GaN barrier in the laser heterostructure. (b) Schematic of the nanowire laser heterostructure, with the calculated mode profile shown alongside. (c) Enhancement in the photoluminescence of the green-emitting disk-in-nanowire sample by surface passivation with parylene. (d) Photoluminescence of GaN nanowires, before and after treatment with ammonium sulfide $(NH_4)_2S_x$.

compliant buffer and accommodates the mismatch strain and resulting dislocations. Achieving emission at longer wavelengths with planar InGaN quantum wells (QWs) is difficult due to the strong polarization field and associated quantum confined Stark effect (QCSE),[29] the presence of compositional inhomogeneities in the ternary alloys with high In composition and the increasing rate of nonradiative recombination due to the lack of confinement of carriers in the in-plane direction in the wells.[30,31] In contrast, (In)GaN nanowires have reduced polarization field due to radial strain relaxation during epitaxy and consequently exhibit smaller radiative lifetimes.[28] Lasers fabricated with these nanowires should, therefore, have reduced threshold current densities compared with planar quantum well lasers emitting at similar wavelengths. Auger recombination coefficients measured in InGaN/GaN disks-in-nanowires are ∼2−3 orders of magnitude smaller than those measured in heteroepitaxial bulk materials.[32] This is important in the context of LED and laser efficiency, which operate at high injection currents. It has also been reported that the surface recombination velocity of GaN nanowires is smaller than that of GaAs by 2 orders of magnitude.[33] Additionally, the nanowire laser heterostructure can be grown on any size silicon wafer available.

In this work, we have realized an edge emitting laser with a GaN nanowire ensemble grown on Si(001) by plasma-assisted molecular beam epitaxy (PA-MBE), with a threshold of 1.72 $kA/cm^2$ compared with typical values of 8−9 $kA/cm^2$ that have been reported for planar green-emitting InGaN/GaN QW


dx.doi.org/10.1021/nl5015603 | Nano Lett. XXXX, XXX, XXX−XXX

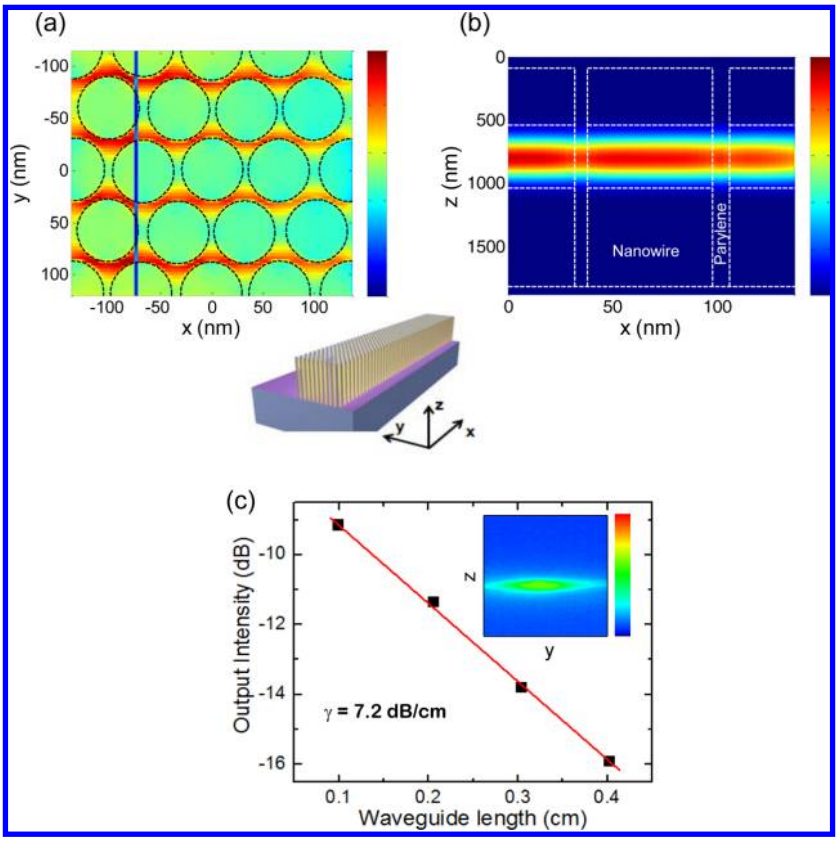


**Figure 2.** Optical field distribution in the (a) $x-y$ and (b) $x-z$ planes, respectively of the nanowire waveguide (with reference to the schematic in panel a). (c) Output intensity of nanowire ridge waveguides, measured with a charged coupled device (CCD) detector, as a function of waveguide length. The inset shows a CCD image from the output facet of the nanowire waveguide.

lasers.[34,35] The p-i-n nanowires have multiple $In_{0.34}Ga_{0.66}N$ disks inserted in the waveguide region, which serve as the gain media. Extensive steady-state and dynamic characterization of the green-emitting ($\lambda$ = 533 nm) devices have been accomplished, from which values of the threshold current, $T_0$, efficiency, differential gain, and small-signal modulation parameters have been derived. The waveguide loss has also been measured. Long-term reliability measurements under continuous wave biasing indicate a lifetime of ~7000 h.

Growth of GaN-based nanowires on silicon has been described in detail in previous reports by us and other authors.[18−20] Nonetheless, the catalyst-free growth of the laser nanostructures by PA-MBE is briefly described here (see Supporting Information). A scanning electron microscope (SEM) image of an as-grown nanowire laser sample grown on Si(001) substrate before fabrication is shown in Figure 1a. A reasonably good uniformity in length is observed in the array of nanowires, which is necessary for laser fabrication. The laser heterostructure incorporated along the nanowire and the role of the various nanowire layers are schematically shown in Figure 1b and are described in the Supporting Information. The high resolution transmission electron microscope (TEM) image shown in the inset of Figure 1a shows one of the $In_{0.34}Ga_{0.66}N$ disks with GaN barrier in the laser heterostructure. The number of $In_{0.34}Ga_{0.66}N$ disks incorporated in the nanowire heterostructure will affect modal gain of the laser. However, increasing the number of disks will increase the threshold current and will cause nonuniform injection of holes among the disk layers due to the heterostructure band line-up. We have included six disk layers in our heterostructures based on optimization of photoluminescence intensity. The thickness of the disks affects the electron hole overlap and hence the emitted light intensity. We have used the optimum value of 2 nm. The disk diameter is ~60 nm. The alloy composition in the disks and their location in the nanowire and composition were derived from energy dispersive X-ray (EDX) spectroscopy. The nanowire aerial density derived from the SEM image of Figure 1a is $2 \times 10^{10}$ $cm^{-2}$. This density has to be very carefully optimized. For a small nanowire density, the volume of the gain material is reduced and the formation and fabrication of the top (p-type) ohmic contact of the laser is rendered more difficult. On the other hand, too large a nanowire density leads to coalescing of the nanowires and the formation of extended defects and stacking faults, which ultimately reduces the radiative efficiency.[36−38] The radiative efficiency is also reduced by surface states of the nanowire. We have investigated the effect of passivation with various compounds on the radiative efficiency and their compatibility with the nanowire laser fabrication process, to be described later. Figure 1c illustrates the enhancement in room temperature photoluminescence from $In_{0.34}Ga_{0.66}N$/GaN disks-in-nanowire upon passivation with parylene. We have determined that the p-contact resistance of GaN:Mg nanowires is reduced upon treatment with ammonium sulfide. Figure 1d shows the improvement in room temperature photoluminescence upon use of ammonium sulfide treatment on these GaN nanowires. Parylene has been used in this study to passivate the nanowires and to planarize the laser cavity.

It is important to know the characteristics of the photon field and the propagation of photon modes in the in-plane direction


dx.doi.org/10.1021/nl5015603 | Nano Lett. XXXX, XXX, XXX−XXX

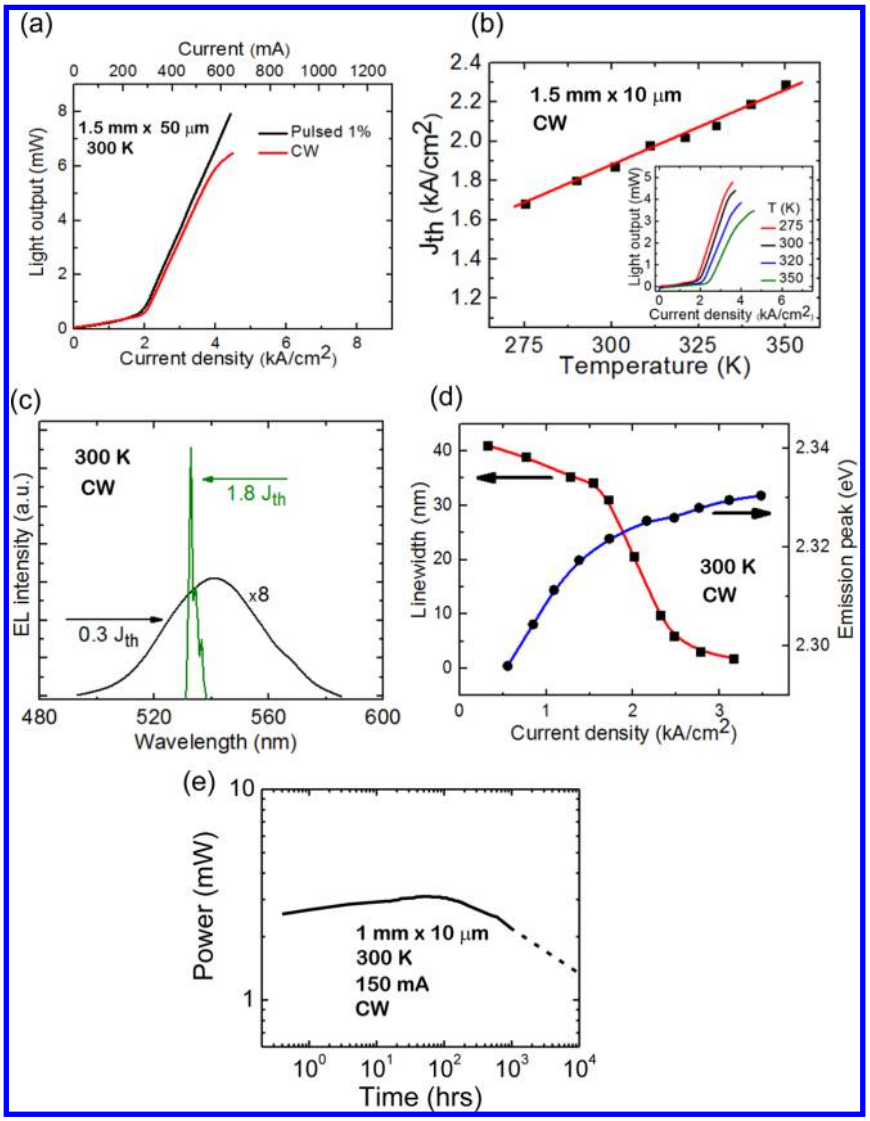


**Figure 3.** (a) Light-current characteristics of a broad area laser. (b) Temperature dependence of the threshold current density in a ridge waveguide laser under continuous wave biasing. The inset shows the measured L-*I* characteristics at different temperatures. (c) Electroluminescence spectra under continuous wave bias above and below threshold. (d) Variation of the emission line width and blueshift of the peak emission with increasing injection current density for the ridge waveguide laser. (e) Output power versus time with an extrapolated lifetime of 7000 h for the output power to be reduced to half the maximum value.

in planar waveguides before proceeding with the fabrication and characterization of nanowire lasers. Ridge-shaped waveguides were fabricated by mesa etching the nanowire laser heterostructure, grown without Si and Mg doping and without the $In_{0.34}Ga_{0.66}N$/GaN disks, in the same way as the edge-emitting lasers (see Supporting Information). Prior to measuring the fabricated waveguides, 3D finite-difference time-domain (FDTD) electromagnetic simulation was performed on the structures in order to understand how the lasing mode will propagate through the nanowire-parylene composite cavity. Nanowire spacing and density will affect mode distribution and scattering and consequently affect macroscopic cavity optical properties of interest to laser operation. The waveguide was modeled as a hexagonal close-packed (HCP) nanowire array with 60 nm nanowire diameter, an average period of 67 nm, and parylene filling the gaps between nanowires as in the fabricated devices. An $Al_{0.11}Ga_{0.89}N$ cladding refractive index of 2.3887, $In_{0.06}Ga_{0.94}N$ waveguide refractive index of 2.4369, and a GaN refractive index of 2.4169 were used for the respective nanowire layers in the simulation. To avoid the possible formation of a photonic crystal and the associated effects, the nanowires were randomly offset from the HCP array sites by a maximum of 2 nm. An absorbing perfectly matched-layer (PML) boundary condition was used in all directions. Figure 2a and b show the cavity field in the $x-y$ and $x-z$ planes, respectively (with reference to the schematic in Figure 2a), in response to a $y$-polarized plane wave modulated by a Gaussian distribution approximating the calculated mode in Figure 1b. The field is continuous over the nanowires, showing no confinement along the cavity length ($x$ axis), indicating that light can freely propagate in the in-plane direction. Hence, the nanowire guide region can be treated as a nanowire-parylene 3D composite with a lower average refractive index of $n_r \sim 2.1$.[39] The localization of a part of the cavity field between the nanowires results from the mutual enhancement of two evanescent fields in close proximity, also observed in slotted guides.[40,41] The discontinuity of the field


dx.doi.org/10.1021/nl5015603 | *Nano Lett.* XXXX, XXX, XXX−XXX

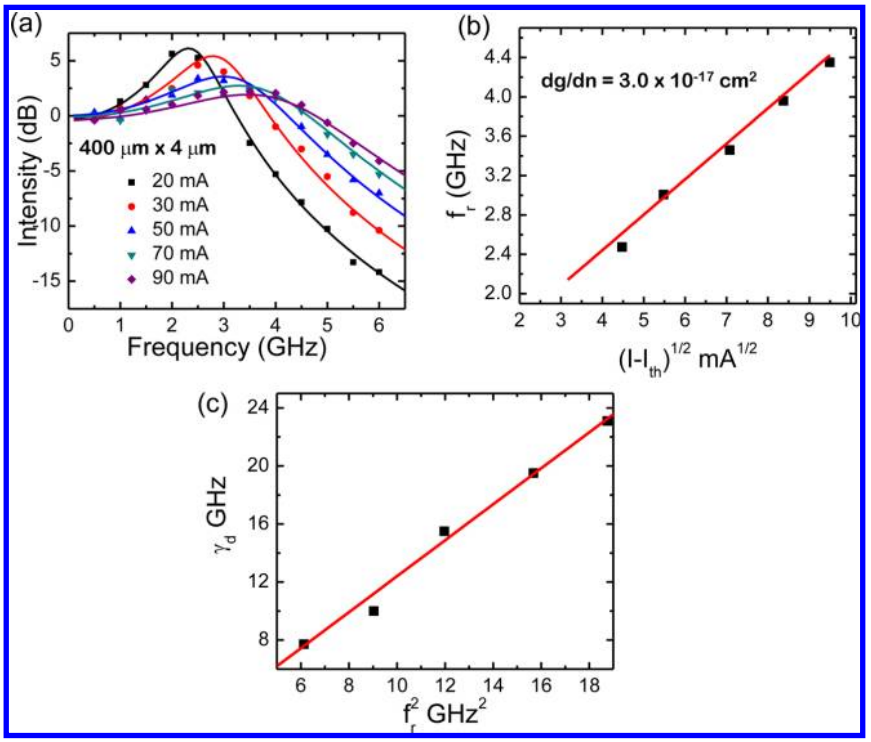


**Figure 4.** (a) Measured small-signal modulation response of a 400 $\mu$m × 4 $\mu$m ridge waveguide laser at 300 K for varying dc injection current values. The data are analyzed to derive the resonance frequency $f_r$ and damping factor $\gamma_d$. (b) Plot of $f_r$ versus square root of injection current. The differential gain is derived from the slope of this plot. (c) Plot of $\gamma_d$ versus square of resonance frequency. The gain compression factor $\varepsilon$ is derived from the slope of this plot.

observed in the $y$ direction is an artifact of the $y$-polarized source used in the simulation.

The propagation loss, including the scattering loss and substrate leakage, in nanowire waveguides was obtained from transmission measurements on ridge waveguides of different length and having a fixed width of 10 $\mu$m. The waveguides were end-fired with light from a 532 nm laser focused to a 10 $\mu m^2$ spot. It may be noted that the sub-bandgap (2.33 eV) excitation will be freely transmitted in the nanowire waveguide wherein the smallest bandgap material is the $In_{0.06}Ga_{0.94}N$ waveguide ($E_g$ = 3.12 eV). The output intensity was measured with a charged coupled device (CCD) detector. The measured output intensity as a function of guide length is plotted in Figure 2c, from which a loss of $\gamma$ = 7.2 dB/cm is derived. This value is of the same order as those of bulk III-nitride semiconductor waveguides,[42,43] in spite of the fact that there is no $Al_{0.11}Ga_{0.89}N$ upper cladding layer. The inset shows a CCD image from the output facet of the nanowire waveguide.

The as-grown nanowire samples are planarized and passivated with parylene, followed by an ammonium sulfide treatment to reduce the p-contact resistance. Ridge waveguide (4−10 $\mu$m ridge width) and broad area lasers (50 $\mu$m wide) are defined by standard photolithography and dry-etching. Ni/Au/ITO and Al are deposited by physical vapor deposition (PVD) as the contacts to the p-GaN and n-Si, respectively. The Si substrate is cleaved and the nanowire/parylene facets are polished by focused ion beam etching, followed by $SiO_2/TiO_2$ Distributed Bragg reflector (DBR) deposition to enhance facet reflectivity. The laser is schematically shown in Figure 1b together with the calculated guided-mode profile, assuming that the space between the nanowires is filled with parylene. Measurements were made on the lasers at room temperature with continuous wave bias (see Supporting Information). The output power versus current, or light-current (L-$I$), characteristics of a broad area device are shown in Figure 3a. The output is measured from the low reflectivity facet. The threshold current density $J_{th}$= 1.76 kA/cm$^2$ and the maximum measured output power from a single facet is 6.5 mW. The slope efficiency of the output is 1.15% (0.03 W/A). Pulsed bias measurements have been made on the same device and the measured L-$I$ characteristics are also shown in Figure 3a. The threshold current density, maximum measured power, and slope efficiency from these data are 1.72 kA/cm$^2$, 8 mW, and 1.3%, respectively. The temperature dependence of the threshold current of a 10 $\mu$m ridge waveguide laser is shown in Figure 3b. The corresponding L-$I$ characteristics are shown in the inset. A value of the temperature coefficient $T_0$ = 232 K, in accordance with the relation $J_{th}(T) = J_{th}(0)\exp(T/T_0)$, is derived. An almost identical value of $T_0$ was measured for green-emitting self-organized quantum dot lasers.[44] The large value of $T_0$ reflects small carrier leakage and a negligible rate of Auger recombination. The values of $J_{th}$ at room temperature quoted above are significantly smaller than those reported for quantum well devices[34,35,45−49] and are comparable to that measured in a green-emitting InGaN/GaN self-organized quantum dot laser.[44,50] The laser output is TE-polarized in the in-plane direction (see Supporting Information).

The electroluminescence (EL) spectrum of a ridge waveguide laser biased above threshold is shown in Figure 3c. The EL spectrum measured in the same device below threshold is also shown alongside. The variation of the emission line width and the blueshift of the peak emission with increasing injection are plotted in Figure 3d. The smallest recorded line width is 8 Å, and the total blueshift of the peak is 8 nm. The corresponding polarization field is calculated to be 618 kV/cm, which is significantly lower than that reported for


dx.doi.org/10.1021/nl5015603 | Nano Lett. XXXX, XXX, XXX−XXX

comparable quantum wells.[51] The lower polarization field is a result of the strain relaxation during epitaxy of the nanowires. A preliminary investigation of the long-term reliability of the nanowire lasers was made by observing the change in output power of a 1 mm × 10 $\mu$m ridge waveguide laser under a constant continuous wave bias of 150 mA. The threshold current of this laser is 70 mA. The result is shown in Figure 3e. An extrapolated lifetime of ~7000 h, at which the output power is expected to be reduced to half of its peak value (3 mW), is derived. To the best of our knowledge, such reliability data has not been reported for any other laser on silicon.

The modal gain of a 10 $\mu$m ridge waveguide laser was measured by the Hakki–Paoli technique[52] (see Supporting Information). The emission spectra for increasing injection are recorded (with a spectral resolution of 0.3 nm) until the threshold is reached, when the spectrum is characterized by a succession of peaks and valleys corresponding to the longitudinal modes. Analysis of this data yields the spectral gain and a peak net modal gain at threshold, $\Gamma g \sim 24$ cm$^{-1}$ is derived. This value compares well with those of calculated gain spectra for $In_{0.27}Ga_{0.73}N$ self-organized quantum dots of base width and height equal to 50 and 3 nm, respectively, in a green-emitting laser.[44]

Measurement of the dynamic characteristics of a laser by direct bias modulation can provide a host of important information. For example, the lasers described here could be directly modulated on a CMOS chip for on-chip communication, without the need for an external modulator. Small-signal modulation experiments provide information regarding the differential gain, gain compression, and other hot-carrier related effects. Measurements were made on 4 $\mu$m ridge waveguide $In_{0.34}Ga_{0.66}N$ disk-in-nanowire lasers of 400 $\mu$m length at room temperature using a 40 GHz high speed detector and electrical spectrum analyzer. The measured response was calibrated for the losses due to cable, connectors, bias network, and dc-blocking capacitor. The modulation response as a function of dc bias current is shown in Figure 4a. The measured data have been analyzed with the small-signal response

$$|R(f)|^2 \propto \frac{1}{(f^2 - f_r^2)^2 + \left(\frac{\gamma_d}{2\pi}\right)^2 f^2} \quad (1)$$

where $f_r$ is the resonance frequency and $\gamma_d$ is the damping factor. A −3 dB modulation bandwidth, $f_{-3\,dB} = 5.8$ GHz was measured for the highest current bias of 90 mA. Figure 4b shows a plot of $f_r$ versus $(I-I_{th})^{1/2}$. The differential gain can be derived from the slope of this plot in accordance with the relation

$$f_r = \frac{1}{2\pi}\left[\frac{v_g \Gamma (I - I_{th})\frac{dg}{dn}\eta_i}{V_{act} q}\right]^{1/2} \quad (2)$$

where $v_g$ is the photon group velocity and $V_{act}$ is the active volume of the gain medium. A value of $dg/dn = 3 \times 10^{-17}$ cm$^2$ is derived from the plot of Figure 4b. Under gain compression limited modulation conditions $\gamma_d$ is related to $f_r$ by the approximate relation $\gamma_d = Kf_r^2$, where $K$ is a measure of the damping related bandwidth and is given by $K \cong 4\pi^2((\in)/(v_g(dg)/(dn)) + \tau_p)$ where $\varepsilon$ is the gain compression factor and $\tau_p$ is the cavity photon lifetime. The plot of $\gamma_d$ versus $f_r^2$ is illustrated in Figure 4c. The value of $K$ derived from the slope is 1.24 ns from which a value of $\varepsilon = 1.22 \times 10^{-17}$cm$^3$ is derived. This value is relatively small, confirming that hot carrier effects do not play any significant role in the operation of the nanowire lasers.[53]

The monolithic nanowire lasers described here are epitaxially grown on Si(001) substrates and are therefore compatible with mainstream Si CMOS technology. Although we have demonstrated a visible laser here, emission into the near-infrared up to ~1.9 $\mu$m is possible by increasing the indium fraction in the $In_xGa_{1-x}N$ disks. Alternative cladding, such as lattice matched $In_{0.18}Al_{0.82}N$ on GaN, will need to be investigated in order to confine the optical mode at these longer wavelengths. Photonic integrated circuits consisting of these longer wavelength lasers with Si waveguides would also be possible with near IR devices, along with front-end photoreceivers (Ge or SiGe detector integrated with amplifier[54]) to form an optical communication link. Currently, visible lasers are grown on extremely expensive GaN substrates. We present extensive data here showing that the nanowire lasers have performance characteristics comparable to or surpassing those of devices grown on GaN. This is due to the extremely low density of extended defects and a small polarization field in the nanowires.

## ■ ASSOCIATED CONTENT

### Supporting Information

Additional information regarding the methods, output polarization, and gain measurements. This material is available free of charge via the Internet at http://pubs.acs.org.

## ■ AUTHOR INFORMATION


### Corresponding Author

*P. Bhattacharya. E-mail :pkb@eecs.umich.edu.


### Notes

The authors declare no competing financial interest.

## ■ ACKNOWLEDGMENTS


The work was supported by the National Science Foundation (MRSEC program) under Grant DMR-1120923 and by the King Abdullah University of Science and Technology, Kingdom of Saudi Arabia, under Grant CRG-1-2012-001-010-MIC. T.F. and E.S. acknowledge support provided by National Science Foundation Graduate Research Fellowships. Epitaxial growth and device fabrication were done in the Lurie Nanofabrication Facility, a member of the National Nanotechnology Infrastructure Network funded by the National Science Foundation.


## ■ REFERENCES


(1) Jalali, B.; Fathpour, S. *J. Lightwave Technol.* **2006**, *24*, 4600–4615.
(2) Soref, R. *IEEE J. Sel. Top. Quantum Electron.* **2006**, *12*, 1678–1687.
(3) Mi, Z.; Yang, J.; Bhattacharya, P.; Qin, G.; Ma, Z. *Proc. the IEEE* **2009**, *97*, 1239–1249.
(4) Liang, D.; Bowers, J. E. *Nat. Photonics* **2010**, *4*, 511–517.
(5) Chen, H. Z.; Ghaffari, A.; Wang, H.; Morkoc, H.; Yariv. *Opt. Lett.* **1987**, *12*, 812–813.
(6) Mi, Z.; Bhattacharya, P.; Yang, J.; Pipe, K. P. *Electron. Lett.* **2005**, *41*, 13.
(7) Liu, A. Y.; Zhang, C.; Norman, J.; Snyder, A.; Lubyshev, D.; Fastenau, J. M.; Liu, A. W. K.; Gossard, A. C.; Bowers, J. E. *Appl. Phys. Lett.* **2014**, *104*, 041104.
(8) Wang, T.; Liu, H.; Lee, A.; Pozzi, F.; Seeds. *Opt. Express* **2011**, *19*, 11381–11386.
(9) Kunert, B.; Zinnkann, S.; Volz, K.; Stolz, W. *J. Cryst. Growth* **2008**, *310*, 4776–4779.

(10) Cerutti, L.; Rodriguez, J. B.; Tournie, E. GaSb-Based Laser. *IEEE Photonics Technol. Lett.* **2010**, *22*, 553−555.
(11) Camacho-Aguilera, R. E.; Cai, Y.; Patel, N.; Bessette, J. T.; Romagnoli, M.; Kimerling, L. C.; Michel, J. *Opt. Express* **2012**, *20*, 11316−11320.
(12) Fang, A. W.; Park, H.; Cohen, O.; Jones, R.; Paniccia, M. J.; Bowers, J. E. *Opt. Express* **2006**, *14*, 9203−9210.
(13) Liang, D.; Roelkens, G.; Baets, R.; Bowers, J. E. *Materials* **2010**, *3*, 1782−1802.
(14) Tanabe, K.; Watanabe, K.; Arakawa, Y. *Sci. Rep.* **2010**, *2*, 349−1−6.
(15) Duan, G. H.; Jany, C.; Liepvre, A. L.; Provost, J.-G.; Make, D.; Lelarge, F.; Lamponi, M.; Poingt, F.; Fedeli, J. M.; Messaoudene, S.; Bordel, D.; Brision, S.; Keyvaninia, S.; Roelkens, G.; Thourhout, D. V.; Thomson, D. J.; Gardes, F. Y.; Reed, G. T. *ECOC Tech. Dig.* **2012**.
(16) Tanaka, S.; Jeong, S. H.; Sekiguchi, S.; Kurahashi, T.; Tanaka, Y.; Morito, K. *Opt. Express* **2012**, *20*, 28057−28069.
(17) Campenhout, J. V.; Rojo-Romeo, P.; Regreny, P.; Seassal, C.; Thourhout, D. V.; Verstuyft, S.; Cioccio, L. D.; Fedeli, J.-M.; Lagahe, C.; Baets, R. *Opt. Express* **2007**, *15*, 6744−6749.
(18) Guo, W.; Banerjee, A.; Bhattacharya, P.; Ooi, B. S. *Appl. Phys. Lett.* **2011**, *98*, 193102.
(19) Calarco, R.; Meijers, R. J.; Debnath, R. K.; Stoica, T.; Sutter, E.; Luth, H. *Nanolett.* **2007**, *7*, 2248−2251.
(20) Calleja, E.; Ristic, J.; Garrido, S. F.; Cerutti, L.; Garcia, M. A. S.; Grandal, J.; Trampert, A.; Jahn, U.; Sanchez, G.; Griol, A.; Sanchez, B. *Phys. Status Solidi B* **2007**, *244*, 2816−2837.
(21) Ristic, J.; Calleja, E.; Garrido, S. F.; Cerutti, L.; Trampert, A.; Jahn, U.; Ploog, K. H. *J. Cryst. Growth* **2008**, *310*, 4035−4045.
(22) Kishino, K.; Kikuchi, A.; Sekiguchi, H.; Ishizawa, S. *Proc. SPIE* **2007**, *6473*, 64730T.
(23) Nguyen, H. P. T.; Cui, K.; Zhang, S.; Fathololoumi, S.; Mi, Z. *Nanotechnology* **2011**, *22*, 445202.
(24) Jahangir, S.; et al. *Appl. Phys. Lett.* **2013**, *102*, 071101.
(25) Chen, H. Y.; Lin, H. W.; Shen, C. H.; Gwo, S. *Appl. Phys. Lett.* **2006**, *89*, 243105.
(26) Geelhaar, L.; et al. *IEEE J. Sel. Top. Quantum Electron.* **2011**, *17*, 878−888.
(27) Cerutti, L.; Ristic, J.; Garrido, S. F.; Calleja, E.; Trampert, A.; Ploog, K. H.; Lazic, S.; Calleja, J. M. *Appl. Phys. Lett.* **2006**, *88*, 213114.
(28) Guo, W.; Zhang, M.; Banerjee, A.; Bhattacharya, P. *Nanolett.* **2010**, *10*, 3355−3359.
(29) Huang, C. F.; Lu, C. F.; Tang, T. Y.; Huang, J. J.; Yang, C. C. *Appl. Phys. Lett.* **2007**, *90*, 151122.
(30) Cho, Y. H.; Gainer, G. H.; Fischer, A. J.; Song, J. J.; Keller, S.; Mishra, U. K.; DenBaars, S. P. *Appl. Phys. Lett.* **1998**, *73*, 1370.
(31) Naranjo, F. B.; García, M. A. S.; Calle, F.; Calleja, E.; Jenichen, B.; Ploog, K. H. *Appl. Phys. Lett.* **2002**, *80*, 231.
(32) Guo, W.; Zhang, M.; Bhattacharya, P.; Heo, J. *Nano Lett.* **2011**, *11*, 1434.
(33) Schlager, J. B.; Bertness, K. A.; Blanchard, P. T.; Robins, L. H.; Roshko, A.; Sanford, N. A. *J. Appl. Phys.* **2008**, *103*, 124309.
(34) Queren, D.; Avramescu, A.; Brüderl, G.; Breidenassel, A.; Schillgalies, M.; Lutgen, S.; Strauß, U. *Appl. Phys. Lett.* **2009**, *94*, 081119.
(35) Avramescu, A.; Lermer, T.; Müller, J.; Tautz, S.; Queren, D.; Lutgen, S.; Strauß, U. *Appl. Phys. Lett.* **2009**, *95*, 071103.
(36) Consonni, V.; Knelangen, M.; Jahn, U.; Trampert, A.; Geelhaar, L.; Riechert, H. *Appl. Phys. Lett.* **2009**, *95*, 241910.
(37) Lefebvre, P.; Garrido, S. F.; Grandal, J.; Ristic, J.; Garcıa, M. A. S.; Calleja, E. *Appl. Phys. Lett.* **2011**, *98*, 083104.
(38) Grossklaus, K. A.; Banerjee, A.; Jahangir, S.; Bhattacharya, P.; Millunchick, J. M. *J. Cryst. Growth* **2013**, *371*, 142−147.
(39) Heo, J.; Jahangir, S.; Xiao, B.; Bhattacharya, P. *Nano Lett.* **2013**, *13*, 2376−2380.
(40) Baehr-Jones, T.; Hochberg, M.; Walker, C.; Scherer. *Appl. Phys. Lett.* **2005**, *86*, 081101.
(41) Wang, G.; Baehr-Jones, T.; Hochberg, M.; Scherer. *Appl. Phys. Lett.* **2007**, *91*, 143109.
(42) Piprek, J.; Nakamura, S. *IEE Proc.: Optoelectron.* **2002**, *149*, 145−151.
(43) Banerjee, A.; Frost, T.; Stark, E.; Bhattacharya, P. *Appl. Phys. Lett.* **2012**, *101*, 041108.
(44) Zhang, M.; Banerjee, A.; Lee, C. S.; Hinckley, J. M.; Bhattacharya, P. *Appl. Phys. Lett.* **2011**, *98*, 221104.
(45) Lin, Y. D.; Yamamoto, S.; Huang, C. Y.; Hsiung, C. L.; Wu, F.; Fujito, K.; Ohta, H.; Speck, J. S.; DenBaars, S. P.; Nakamura, S. *Appl. Phys. Express* **2010**, *3*, 082001.
(46) Avramescu, A.; Lermer, T.; Müller, J.; Eichler, C.; Bruederl, G.; Sabathil, M.; Lutgen, S.; Strauss, U. T. *Appl. Phys. Lett.* **2010**, *3*, 061003.
(47) Müller, J.; Strauß, U.; Lermer, T.; Brüderl, G.; Eichler, C.; Avramescu, A.; Lutgen, S. *Phys. Status Solidi* **2011**, *208*, 1590−1592.
(48) Huang, C. Y.; Hardy, M. T.; Fujito, K.; Feezell, D. F.; Speck, J. S.; DenBaars, S. P.; Nakamura, S. *Appl. Phys. Lett.* **2011**, *99*, 241115.
(49) Ueno, M.; Yoshizumi, Y.; Enya, Y.; Kyono, T.; Adachi, M.; Takagi, S.; Tokuyama, S.; Sumitomo, T.; Sumiyoshi, K.; Saga, N.; Ikegami, T.; Katayama, K.; Nakamura, T. *J. Cryst. Growth* **2011**, *315*, 258−262.
(50) Bhattacharya, P.; Banerjee, A.; Frost, T. *Proc. SPIE* **2013**, *8640*, 86400J.
(51) Jho, Y. D.; Yahng, J. S.; Oh, E.; Kim, D. S. *Phys. Rev. B: Condens. Matter Mater. Phys.* **2002**, *66*, 035334.
(52) Hakki, B. W.; Paoli, T. L. *J. Appl. Phys.* **1975**, *46*, 1299.
(53) Gomatam, B. N.; DeFonzo, A. P. *IEEE J. Quantum Electron.* **1990**, *26*, 1689−1704.
(54) Qasaimeh, O.; Zhenqiang, M.; Bhattacharya, P.; Croke, E. T. *J. Lightwave Technol.* **2000**, *18* (11), 1548.